ACS APPLIED NANO MATERIALS

www.acsanm.org Article

Comprehensive Characterization of Nanosized Extracellular Vesicles from Central and Peripheral Organs: Implications for Preclinical and Clinical Applications

Subhash Chand, Ala Jo, Neetha Nanoth Vellichirammal, Austin Gowen, Chittibabu Guda, Victoria Schaal, Katherine Odegaard, Hakho Lee, Gurudutt Pendyala, and Sowmya V. Yelamanchili*

Cite This: *ACS Appl. Nano Mater.* 2020, 3, 8906–8919 Read Online

ACCESS | Metrics & More | Article Recommendations | Supporting Information

ABSTRACT: Extracellular vesicles (EVs) are nanosized vesicles that have been garnering a lot of attention for their valuable role as potential diagnostic markers and therapeutic vehicles for a plethora of pathologies. While EV markers from biofluids such as plasma, serum, urine, cerebrospinal fluid, and *in vitro* cell culture-based platforms have been extensively studied, a significant knowledge gap that remains is the characterization of specific organ-derived EVs (ODE). Here, we present a standardized protocol for isolation and characterization of purified EVs isolated from brain, heart, lung, kidney, and liver from rat and postmortem human tissue. Next, using quantitative mass spectrometry-based proteomics, we characterized the respective tissue EV proteomes that identified synaptophysin, caveolin-3, solute carrier family 22 member 2, surfactant protein B, and fatty acid-binding protein 1 as potential markers for the brain, heart, kidney, lung, and liver EV, respectively. These respective tissue-specific markers were further validated using both immunoblotting and a nanoplasmonic platform single EV imaging analysis in the two species. To summarize, our study for the first time using traditional biochemical and high-precision technology platforms provides a valuable proof-of-concept approach in defining specific ODE markers, which could further be developed as potential therapeutic candidates for respective end organ-associated pathologies.

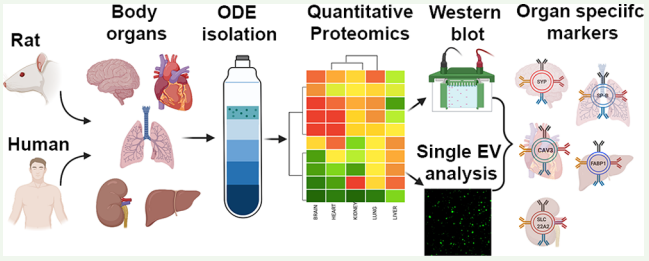

KEYWORDS: *extracellular vesicles, nanovesicles, organ-specific markers, organ-derived extracellular vesicles, nanoplasmonic, quantitative proteomics, single EV imaging*

INTRODUCTION

Extracellular vesicles (EVs) are phospholipid nanovesicles that include (based on their origin or size), apoptotic bodies, microvesicles (MVs), and exosomes and are garnering significant attention as molecules involved in cell−cell communication between cells and regulating the pathophysiology of several diseases.[1−3] EVs carry molecular cargo such as proteins, lipids, and RNA,[4−6] and the molecular composition of the EV cargo generally depends on their cells/tissue of origin. Furthermore, recent works demonstrating the role of EVs as next-generation biomarkers based on their feasibility as therapeutic drug-delivery nanocarriers and in immunotherapy[7,8] have made them exciting candidates for diagnostics and therapeutics in an array of diseases.[9−11] A recent study revealed the use of a quantum dot-based fluorescent immunoassay capable of distinguishing pancreatic cancer patients from healthy controls based on EV as biomarkers.[12] Similarly, assays such as nanoscale fluorescence analysis and cytometric sorting (nanoFACS) techniques have been developed to detect tumor-specific antigens in EVs.[13] Nanoengineered ExoProfile chip has enabled simultaneous detection of up to eight biomarkers from one EV sample to enhance the distinction between early and late-stage cancer diagnosis.[14] Furthermore, plasma-derived exosomes have been analyzed to provide insights into the microRNA cargo profiles in the diagnosis of diseases such as type-1 diabetes mellitus.[15]

Recently, several studies were performed to detect neuronal EVs in plasma in an effort to identify and establish biomarkers for cognitive impairment in human immunodeficiency virus (HIV) infection and neurodegenerative diseases.[16,17] In addition to plasma,[18,19] serum and cerebrospinal fluid-derived EVs have also been studied to reveal potential diagnostic and prognostic biomarkers in glioma patients.[20−23] Because body fluids (*e.g.*, blood plasma, urine, and cerebrospinal fluid) can be serially obtained at different disease stages, isolation of EVs

Received: June 16, 2020
Accepted: August 6, 2020
Published: August 6, 2020

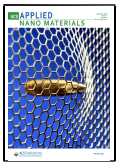

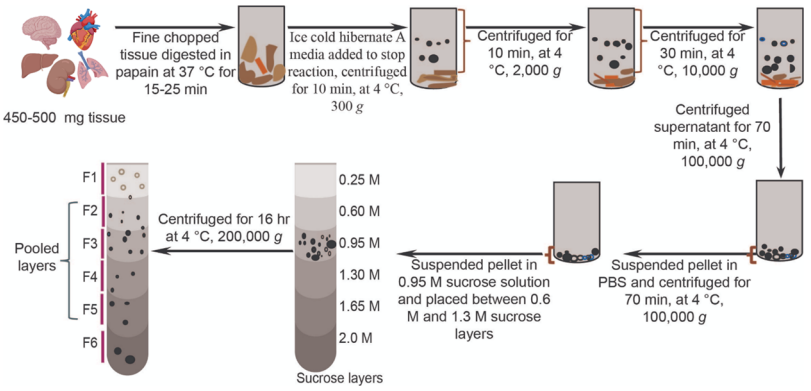

Figure 1. Schematic of the isolation procedure of EVs from different rat tissues. Tissue (~450 mg) from the respective organs was sliced in small pieces and digested at 37 °C for 15−25 min. Cold Hibernate A quenched the reaction it was centrifuged sequentially at 300*g* and 2000*g* for 10 min at 4 °C, and 10,000*g* for 30 min at 4 °C. Further, the supernatant was passed through a 0.20 μm filter and was centrifuged at 100,000*g* for 70 min at 4 °C. EV pellet was suspended in PBS and again centrifuged at 100,000*g* for 70 min at 4 °C. Next, the EV pellet was suspended in 2 mL of 0.95 M sucrose solution, layered in between 0.60 and 1.30 M sucrose layers and centrifuged at 200,000*g* for 16 h at 4 °C. The figure has been created using Adobe Illustrator and Biorender.com.

from them lend a distinct advantage of providing real-time monitoring of the progression of the illness[24] and thus making them attractive targets for diagnostic applications.[25−27]

Despite the many advantages of body fluid-associated EVs as potential biomarkers, a significant limitation is the identification of organ-specific EV markers, which can offer more depth in understanding the respective end organs and associated pathologies. Most studies have been conducted on cell lines or biofluids with little understanding of how organ-specific EVs are expressed *in situ*. Although we and others have reported the feasibility of EV isolation from brain[28−33] and liver tissues,[29] till date, there is no existing literature comparing EVs from different organs including identification of definitive organ-specific EV markers. To address these challenges, the current study performed a comprehensive analysis of the respective tissue EV proteomes from the brain, heart, lung, kidney, and liver from both preclinical (rat) and clinical (postmortem human tissues). We identified synaptophysin (SYP), caveolin-3 (CAV3), solute carrier family 22 member 2 (SLC22A2), surfactant protein B (SP-B), and fatty acid-binding protein 1 (FABP1) as potential markers for the brain, heart, kidney, lung, and liver EV, respectively. These respective tissue-specific markers were further validated using both immunoblotting and a nanoplasmonic platform single EV imaging analysis in the two species. To summarize, our study for the first time, using traditional biochemical and high-precision technology platforms provides a valuable proof-of-concept approach in defining specific organ-derived EV (ODE) markers, which further could be developed as potential therapeutic candidates for respective end organ-associated pathologies.

RESULTS AND DISCUSSION

Isolation and Characterization of EVs from Body Organs. One main goal of this study was to establish a standard protocol for isolation and characterization of EVs isolated from different organ tissues. Figure 1 shows the scheme for isolating ODEs, with minor modifications of previously published protocols.[31,32] Both transmission electron microscopy (TEM) and nanoparticle tracking analysis (NTA) revealed that EVs purified from nonperfused rat organs displayed sizes between ~70 and 250 nm (Figure 2A). Interestingly, lung-derived EVs displayed characteristic membrane protrusions that resemble plasma membrane budding (Figure 2A). Next, we characterized four EV protein markers (Hsp-70, flotillin-1, CD63, and CD81) and a negative marker (calnexin) by western blot on rat ODEs and in whole tissue lysates. Figure 3A shows the expression profile of all the EV makers validated in the different ODEs and tissue lysates. Expression of Hsp-70 was observed in the brain, heart, lung, and liver but not in the kidney-derived EVs, while flotillin-1 (Flot-1) was detected in all except the lung-derived EVs. Flot-1 has been shown to be ubiquitously present in all EV types; however, it is less enriched in the small EVs.[34] Its absence in lung-derived EVs indicates that there may be a different biogenesis mechanism in lungs and could also explain its unique morphological characteristic. These markers were, however, detected in all the tissue lysates from the different organs. The tetraspanins CD63 and CD81 were detected in all ODEs. Lastly, the negative maker calnexin was expressed only in the tissue lysates of the different organs. In summary, our western blot analysis showed positive protein bands for at least three classical EV markers for all organs (brain, heart, kidney, lung, and liver). Further, we ascertained if perfusion of animals with saline prior to harvesting tissues affects ODE isolations. Interestingly, we did not observe any differences in total EV protein yield when comparing perfused and nonperfused organs (see Table S1). TEM and western blot analysis revealed no major differences in size and EV marker expression between nonperfused and perfused ODE (Figures S1 & S2). Furthermore, western blot results also revealed similar EV marker profiles as seen with ODE isolated from nonperfused animals. These data corroborate with a recent work conducted on brain-derived EVs, where the authors failed to see significant differences in total EV number from perfused and nonperfused brains.[35] Presence of heterogeneous EV sizes could reveal the presence of various EV subtypes in organs. Generally, the tetraspanin markers CD63 and CD81 are predominantly present in the smaller-sized EV subtype, exosomes, whereas Flot-1 and Hsp-70 have been shown to be present in other larger-sized EV populations.[34,36] The absence of Flot-1 and Hsp-70 markers from lung and kidney, respectively, indicates the absence of a subset of larger EV population. Overall, the data demonstrates the feasibility, rigor,

https://dx.doi.org/10.1021/acsanm.0c01654
ACS Appl. Nano Mater. 2020, 3, 8906−8919

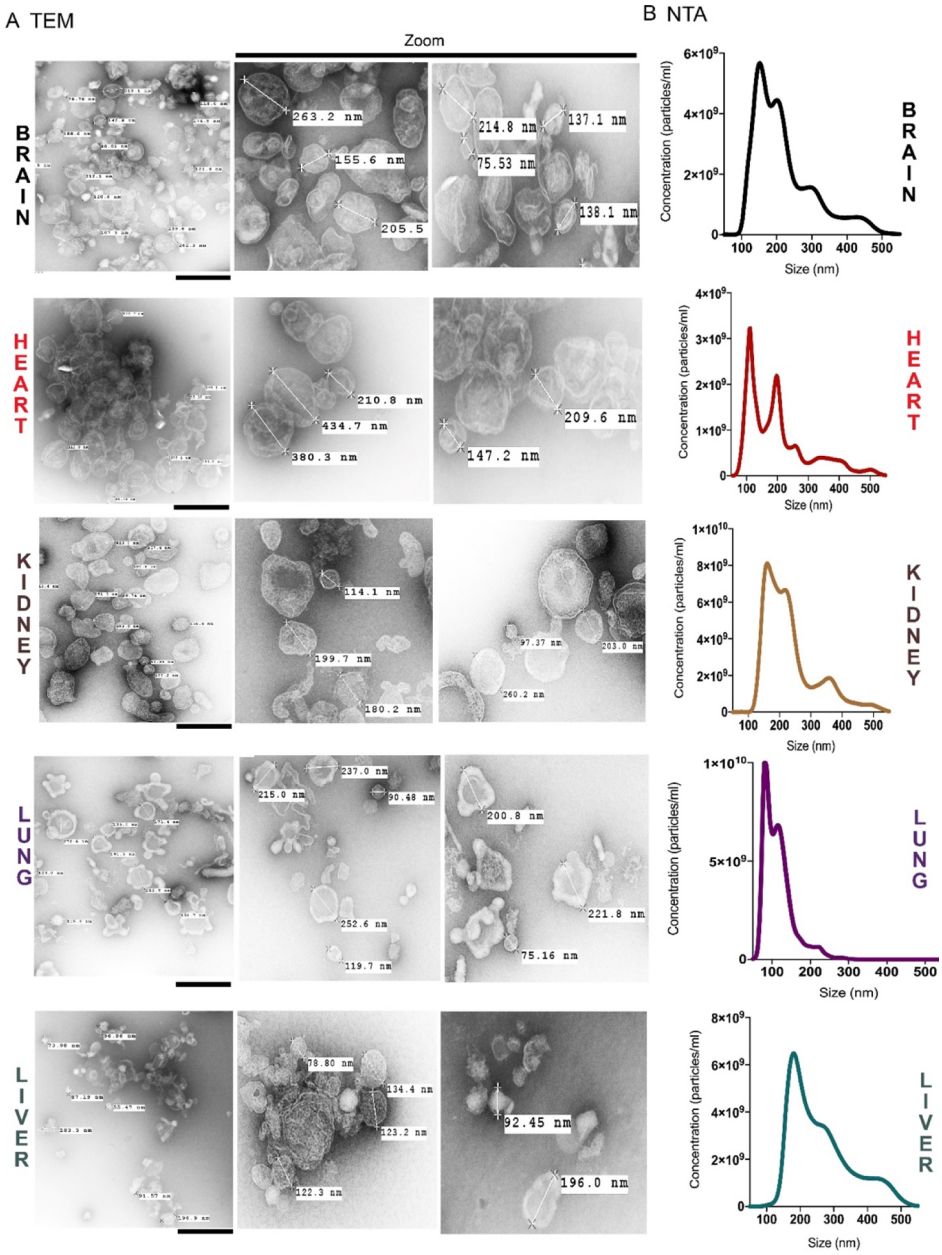

Figure 2. Characterization of EVs isolated from rat tissues. (A) TEM analysis of EVs from rat brain, heart, kidney, lung, and liver. Scale bars, 500 nm. (B) NTA of EV samples isolated from nonperfused rat organs (brain, heart, kidney, lung, and liver).

and reproductivity of isolating ODE from different rat organs in nonperfused and perfused conditions.

Proteomic Analysis of ODEs. It is well-known that EV protein cargo can be used as biomarkers for detection of various diseases such as cancer,[37] neurological,[17] and cardiovascular diseases.[38] To determine the composition of the EV proteome from the different organs, we performed comprehensive profiling of ODEs using quantitative mass spectrometry-based proteomics. Because we did not find major differences in size or markers between the perfused and nonperfused organ isolations, nonperfused rat organs were used for this proteomics study. We analyzed three biological replicates of ODEs isolated from our rat organs. A protein was identified as differentially expressed if the false discovery rate (FDR) (Benjamini and Hochberg's method)-corrected *P*-value was $\leq$0.05, and log 2-fold change was $\geq$1.5. As seen in Figure 3B, principal component analysis (PCA) revealed a distinguishable organ-specific clustering of ODE proteins. Overall, PCA analysis shows that the EV protein contents of various organs are significantly different from each other.

Next, we assessed the differential expression of proteins expressed in ODE isolated from different organs. Proteins identified with at least two unique peptides were included in the downstream differential analysis. Figure 4A(i) shows the number of upregulated proteins in the brain when compared with heart, kidney, lung, and liver EV proteins. We identified a total of 399 EV proteins that were upregulated in brain EVs when compared to the rest of the organs analyzed. Of these, 147 had significantly higher expression across all comparisons (Figure 4A and Table S2). A similar analysis of the heart, kidney, lung, and liver also identified several EV proteins that were highly abundant in one organ compared to the rest analyzed in this study (Figure 4A(ii–v) and Table S2). Functional annotation using the bioinformatic tool, ClueGo,

https://dx.doi.org/10.1021/acsanm.0c01654
ACS Appl. Nano Mater. 2020, 3, 8906–8919

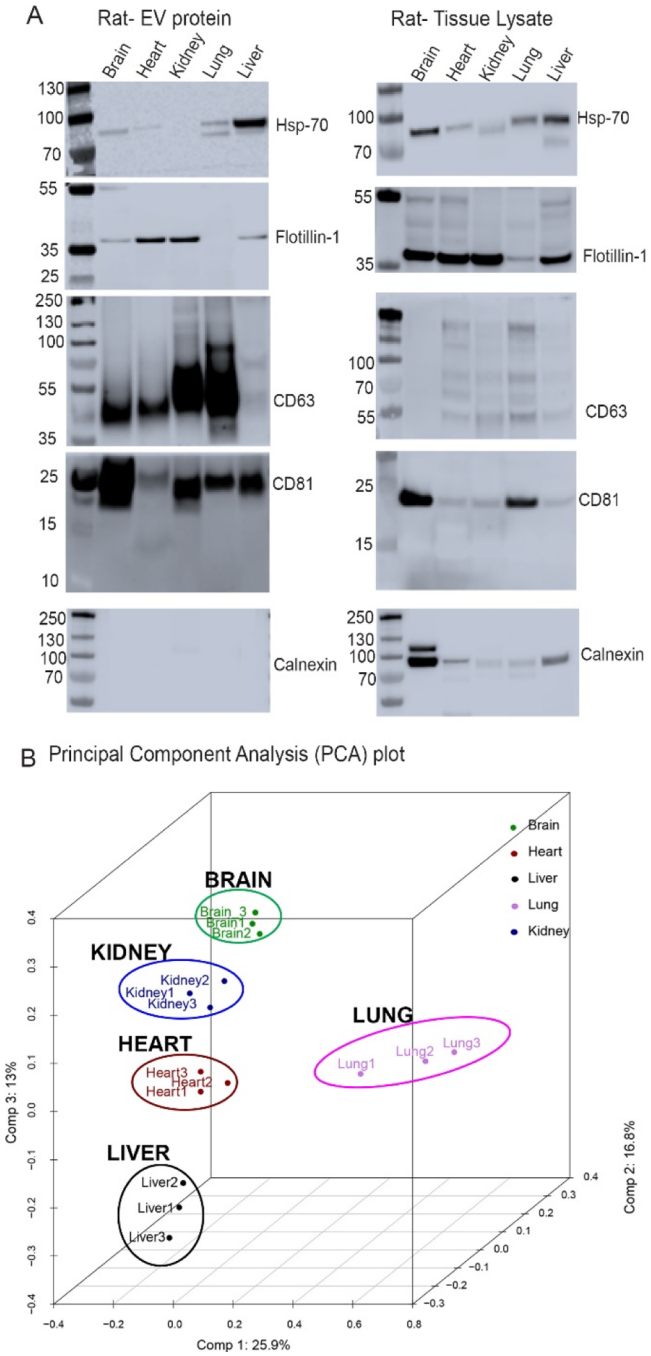

Figure 3. Western blot and PCA of EV purified from rat organs. (A) Left, western blot of EV proteins isolated from rat tissue and right, whole tissue lysate for positive and negative EV markers. (B) 3D-PCA plot of the rat brain, heart, kidney, lung, and liver EV protein samples. Ellipses and shapes show the clustering of the samples. Replicate dots depict the proteomes of the EV from the rat brain (green), heart (red), kidney (blue), lung (violet), and liver (black).

revealed that among the 147 differentially upregulated brain EV proteins, a majority of these were involved in synaptic vesicle recycling, protein/amino acid transport, and neuronal synaptic plasticity (Figure 4B(i)). The majority of heart EV proteins were involved in proton transport and oxidative phosphorylation pathways (Figure 4B(ii)). EV proteins from the kidney (7 groups), lung (8 groups), and liver (5 groups) were enriched with transmembrane transporter activity, regulation of actin filament polymerization, and peroxisome proliferator-activated receptor signaling pathway, respectively (Figure 4B(iii–v)). Bar charts of the data are represented in Figure S3. It is widely accepted in the EV field that most of the cargo content expressed represents proteins or RNA carried in the host cells. It is interesting to note that protein cargos expressed in ODE from organs represent the major proteins (membrane proteins, receptors, and transporters) expressed in that particular organ. For example, brain-derived EVs express largely synaptic membrane proteins and receptors (Figure 4B(i)). Similarly, kidney-derived EVs express mostly transporters, which are abundantly expressed in kidneys (Figure 4B(iii)). In summary, the proteomic analysis of ODEs revealed distinct organ-specific protein signatures.

Identification and Characterization of Organ-Specific Markers. Based on the bioinformatic analysis and normalized spectral count, we characterized the top 25 most abundant ODE proteins (Figure 5 and Table S3). Because high throughout approaches such as proteomics yield a lot of data, it is imperative to validate the identified potential hits. Accordingly, we performed postvalidation of the respective ODE markers by western blot. In our quest to narrow our search for a good organ-specific marker, we first compared the proteins abundant in different organs with the publicly available tissue-enrichment data set (https://v15.proteinatlas.org/tissue). Using this approach, we selected the following ODE markers for the respective organs. Brain: SYP, neural cell adhesion molecule 1 (NCAM1), excitatory amino acid transporter 1 (EAA1), and myelin oligodendrocyte glycoprotein (MOG); heart: CAV3 and cytochrome *c* oxidase subunit 5B (COX5B); kidney: SLC22A2and solute carrier family 12 member 1 (S12A1); lung: SP-B, intercellular adhesion molecule 1 (ICAM1), annexin A5 (ANXA5), and acidic mammalian chitinase (CHIA); and liver: FABP1, glutathione S-transferase Mu 1 (GSTM1), microsomal glutathione S-transferase 1 (MGST1), and 3-β-hydroxysteroid dehydrogenase type 7 (HSD3B7) (Figures 6A(i–v) & S3(A–E)). Following immunoblotting, we confirmed the validation of SYP, CAV3, SLC22A2, SP-B, and FABP1 as a potential brain, heart, kidney, lung, and liver-EV marker, respectively, from nonperfused, perfused ODEs, and whole tissue lysates (Figure 6B). The other markers identified showed either nonspecificity or significant expression in more than one primary organ of interest and, therefore, could not meet the criteria for an organ-specific marker (Figure S4).

Although our results confirmed the presence of one predominant marker, we also found more than one significantly expressed EV protein on ODE. For example, brain, given its complexity in structure and function, is one of the most studied organs in EV biology. EVs can readily cross the blood–brain barrier, making them attractive biomarkers for prognostic and diagnostic purposes for mental disorders.[39] Recent studies have shown some success in identifying a neuron-specific EV marker, L1CAM, in plasma.[40−44] In one recent study, it was shown that cleaved forms of L1CAM could be immunoprecipitated by a biotin-labeled antibody from the brain and sera of HIV-1 transgenic (Tg) rats.[42] They also show that the cleaved forms are enriched in the HIV-1 Tg rats when compared to the wild type. Whether the cleaved forms of L1CAM are found on the surface of the EV or inside is not clear from these studies. In our proteomics screen under physiological conditions, we found that in brain, L1CAM is significantly less expressed than SYP, an enriched neuronal marker (Figure S5). It is important to note that both L1CAM

https://dx.doi.org/10.1021/acsanm.0c01654
ACS Appl. Nano Mater. 2020, 3, 8906−8919

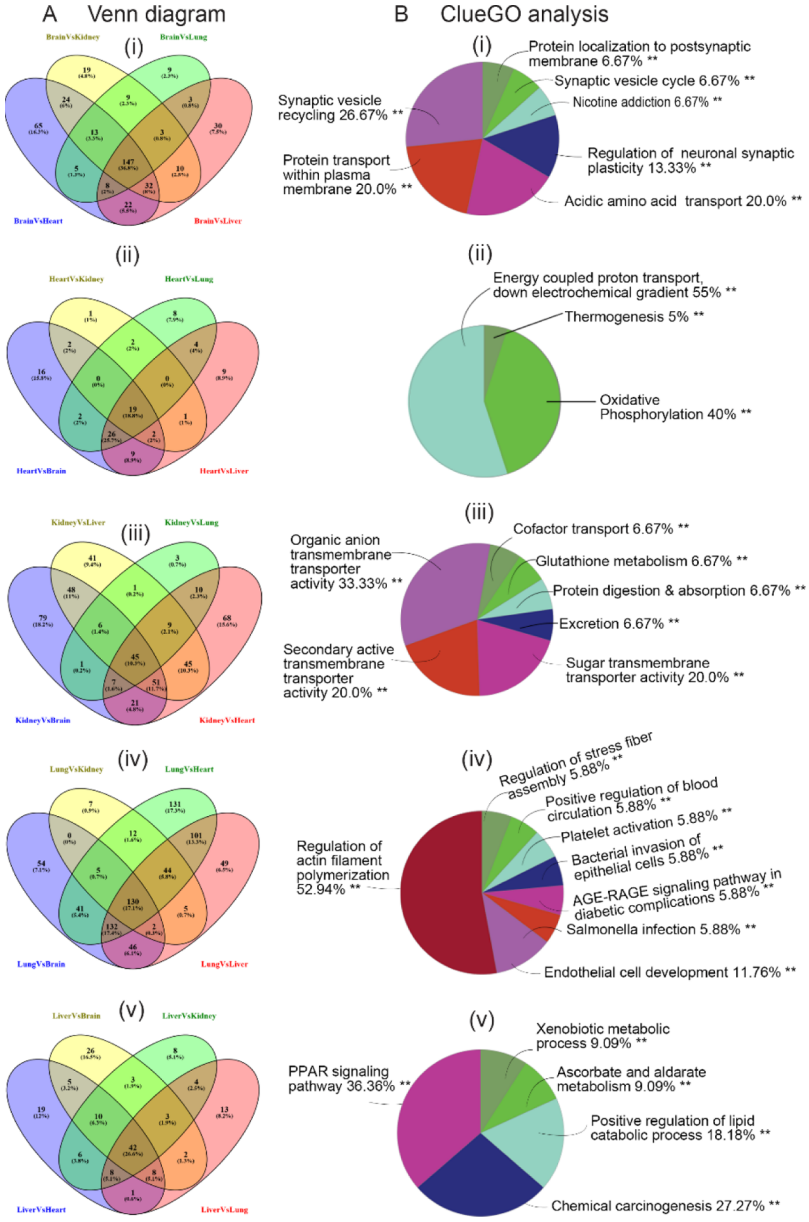

Figure 4. Proteomic analysis of EV contents. (A) Venn diagram showing the upregulated proteins in EVs isolated from the brain (i), heart (ii), kidney (iii), lung (iv), and liver (v) each in comparison with one other tissue. (B) ClueGO analysis of upregulated genes in EVs isolated from different tissues are represented as a pie chart showing the enrichment of functional groups in the brain (i), heart (ii), kidney (iii), lung (iv), and liver (v). The pie chart represents the percentage of known functions of the proteins abundant in each tissue. Data presented are from three independent biological replicates.

and SYP are expressed in other organs as well but highly enriched in the brain. SYP is an integral membrane protein localized to synaptic vesicles and the presynaptic membrane.[45] SYP has been previously shown to be differentially regulated in neuronal-derived exosomes (NDEs) isolated from plasma of individuals with frontotemporal dementia, Alzheimer's disease (AD), and HIV neurological disease.[44,46] Interestingly, another synaptic protein, synaptosomal-associated protein, 25 kDa (SNAP-25), has also been shown to increase in NDEs isolated from serum of AD patients.[47] Further, we detected EAA1 or GLAST in brain EVs. GLAST has been recently reported as a marker for identifying astrocyte-derived EVs in plasma.[48] Another glial-specific marker, S100β was also detected in our proteomics screen.

Similarly, for heart EVs, CAV3 was validated to be a heart-specific EV marker. CAV3 is a cholesterol-binding protein and is one of the main protein components of caveolae and is involved in many cardiovascular processes such as myocardial hypertrophy, myocardial ischemia, and arrhythmogenesis.[49] One recent study showed that CAV3 is present in MVs released from cardiomyocytes.[50] Because of its highest expression in heart EVs when compared to rest of the ODE, CAV3 could be potentially used to isolate heart EVs from peripheral biofluids to determine cardiovascular dysfunction in individuals with heart disease. Intriguingly, organ- or tissue-specific EVs could serve as noninvasive biomarkers to monitor immunologic rejections of transplanted tissues.[51] A recent heart transplant study in mice showed that EVs released from the donor's heart could predict early acute rejection in the

https://dx.doi.org/10.1021/acsanm.0c01654
ACS Appl. Nano Mater. 2020, 3, 8906−8919

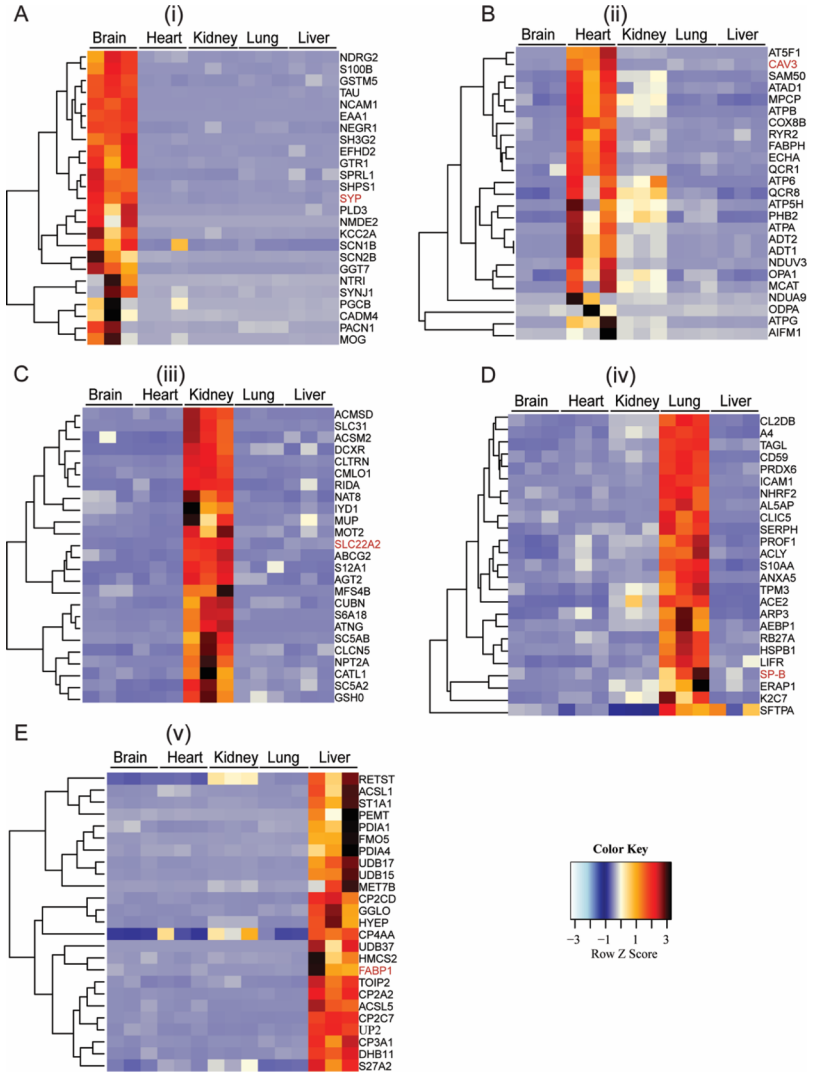

Figure 5. Heatmap of EV proteins. (A–E) Heatmap for top 25 upregulated EV proteins of the brain (A), heart (B), kidney (C), lung (D), and liver (E) in comparison to EV proteins of other organs. Data presented are with FDR correction set at 5% and $P < 0.05$.

host.[52] Alterations in the expression of CAV3 could potentially serve as a biomarker to detect heart-specific alterations. Kidney-specific marker, SLC22A2, is an organic cation transporter 2, which plays an important role in the renal secretion of various cationic compounds.[53−56] Further, EVs isolated from human urine could potentially serve as a noninvasive biomarker for renal dysfunction.[57,58] Lung-derived EV and its associated cargo can be used as a noninvasive biomarker for diagnostic, prognostic, and therapeutic treatment of lung disorders, especially cancer.[59−62] SP-B is a lipophilic protein that is required to facilitate lung inflation and minimize the work of respiration by reducing surface tension in the lung, thus maintaining alveolar stability. Mature SP-B forms are seen in multivesicular bodies, indicating their likely presence on EVs.[63] Circulating immature forms of SP-B (pro-SP-B) were identified as lung-specific biomarkers for alveolar-capillary membrane dysfunction, increased risk of lung cancer, and chronic obstructive pulmonary disease.[64−66] Finally, for the liver, we found FABP1 to be a specific marker. FABP1 is critical for fatty acid metabolism and plays a protective role during oxidative stress, starvation, and infections.[67] Additionally, FABP1 has previously been used as a molecular biomarker in drug-induced liver injury.[68] A recent finding indicated that in patients with type 2 diabetes mellitus, FABP1 is linked to the pathogenesis of the nonalcoholic fatty liver disease.[69] FABP1 plasma levels have shown a positive correlation with body mass index, creatinine levels, waist circumference, and many hepatic diseases.[69] Interestingly, one study reported the presence of FABP1 in exosomes derived from hepatocytes.[70]

Intriguingly, many of the organ-specific EV markers that were identified through our proteomic screening are also invariably enriched in the host tissue and subcellular organelles. For example, liver-specific FABP1 and brain-specific SYP are also found in organelles such as peroxisomes and synaptic vesicles, respectively. However, the isolation of peroxisomes, for instance, uses an entirely different protocol than EV which includes freezing of the density step gradient, a prerequisite for a successful separation.[71] Similarly, synaptic vesicle preparations include breaking of the synaptosome membranes before the high centrifugation step to release synaptic vesicles.[72−76] Hence, the variances in the isolations method largely prevent any organelle contaminations. To summarize, our results conclude that it is imperative to determine more than one organ-specific EV marker in biofluids to discern the EV origin and therefore its relevance to pathogenesis.

https://dx.doi.org/10.1021/acsanm.0c01654
ACS Appl. Nano Mater. 2020, 3, 8906−8919

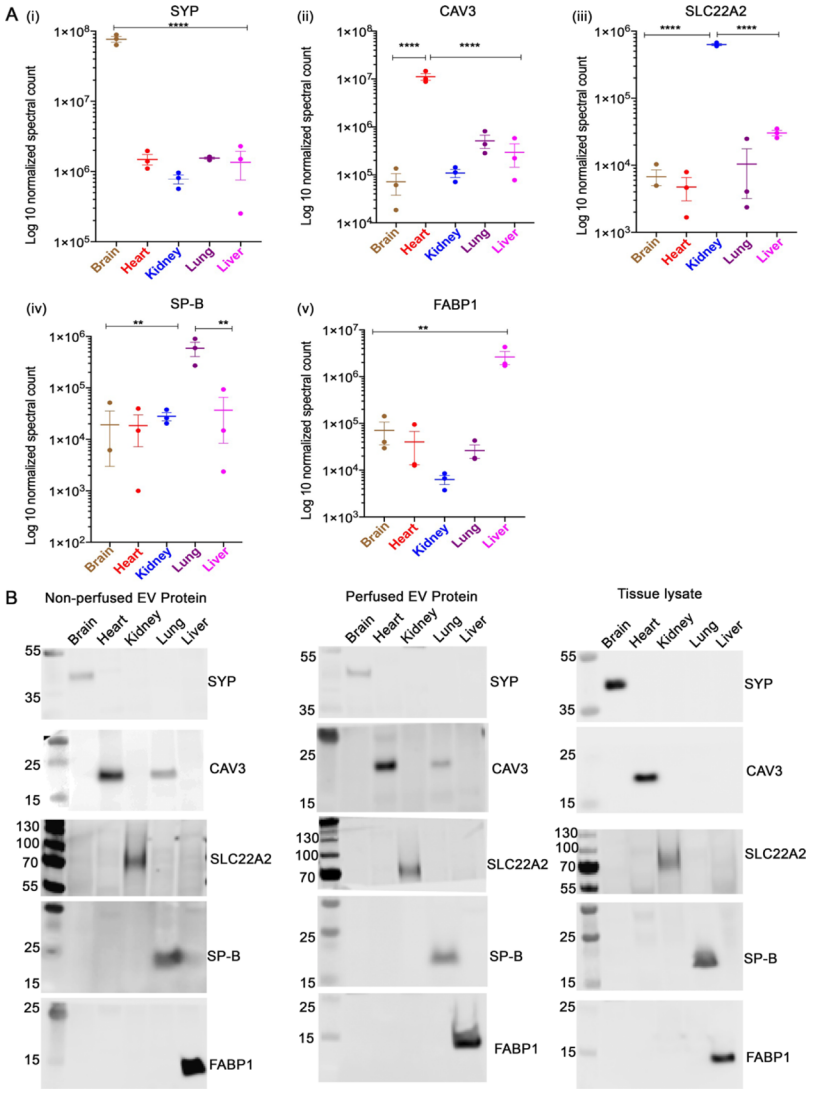

Figure 6. Characterization of organ-specific protein EV markers of different organs. (A) Comparison of SYP (i), CAV3 (ii), SLC22A2 (iii), SP-B (iv), and FABP1 (v) for brain, heart, kidney, lung, and liver EV proteins based on log 10-normalized spectral counts. (B) Western blot analysis of nonperfused and perfused tissue EV, and tissue lysate for brain-specific (SYP), heart-specific (CAV3), kidney-specific (SLC22A2), lung-specific (SP-B), and liver-specific (FABP1) proteins. Data are shown as ± SEM. $^{**}P < 0.01$, $^{***}P < 0.001$, $^{****}P < 0.0001$.

ODE Profiling through Single EV Imaging. In additional to the traditional western blotting, we also validated the specificity of ODE markers by using a nanoplasmonic technology platform: single EV analysis (SEA). SEA technology is capable of robust, multiplexed protein biomarker measurement in individual vesicles. EVs are immobilized inside a microfluidic chamber, and then, on-chip immunostaining and imaging are performed.[77] Here, marker sets that showed the highest selectivity among organs were used: SYP (brain), CAV3 (heart), SLC22A (kidney), SP-B (lung), and FABP1 (liver). We first matched the concentration of ODEs harvested from different organs (1.0×10^{10} EV/mL). These samples were then immunolabeled for fluorescent imaging. As a representative result, Figure 7A shows ODE images with SYP labeling. Overall, the marker expression was dominant only in brain-derived EVs, corroborating the validation from our immunoblotting platform. We further used marker-positive EV numbers as a metric for quantitative comparison (Figure 7B). SYP-labeling imparted a significant contrast between brain-derived EVs and other ODEs. For a given marker, we defined its selectivity as the ratio between marker-positive and -negative EV counts. For SYP, these values were >65. Similarly, we observed high selectivity for other markers (Figure 7C; see Figure S6 for all images); the average selectivity was 30.

Currently available diagnostics are less sensitive and require 10^5 to 10^6 EV per biomarker to measure proteins (*e.g.*, western blot, enzyme-linked immunosorbent assay) or 10^2 to 10^3 EV for the more sensitive methods (μNMR, nPLEX).[77] This newly developed method could be invariably used to isolate and quantitate organ-specific EV changes from biofluids to follow the progression of disease pathology during therapy.

Validation of ODEs from Human Postmortem Tissues. To further extend our preclinical findings from a rat model to a clinical setting, we validated the identified ODE markers in postmortem human tissues. We isolated EV from postmortem human brain, heart, kidney, lung, and liver tissues and performed TEM, NTA, and SEA as performed previously in our rat studies. TEM analysis confirmed that we collected nanoscale vesicles from human organs (Figures 8A and S7). Intriguingly, we obtained less total EV proteins when

https://dx.doi.org/10.1021/acsanm.0c01654
ACS Appl. Nano Mater. 2020, 3, 8906−8919

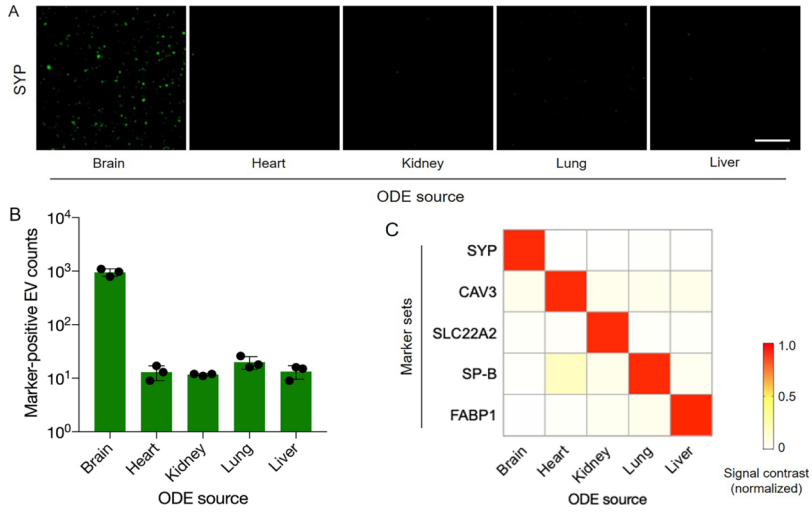

Figure 7. Single EV imaging. (A) Rat ODEs were labeled for the brain-specific surface marker (SYP). Strong positive signal was observed from brain-derived EVs. Scale bar, 20 μm. For other organ-specific markers, see Figure S5. (B) SYP-positive EV numbers were compared. The contrast ratio between brain-derived EVs and other ODEs was >50. (C) Signal contrast among ODE types and organ-specific markers was compared. The data were row-normalized.

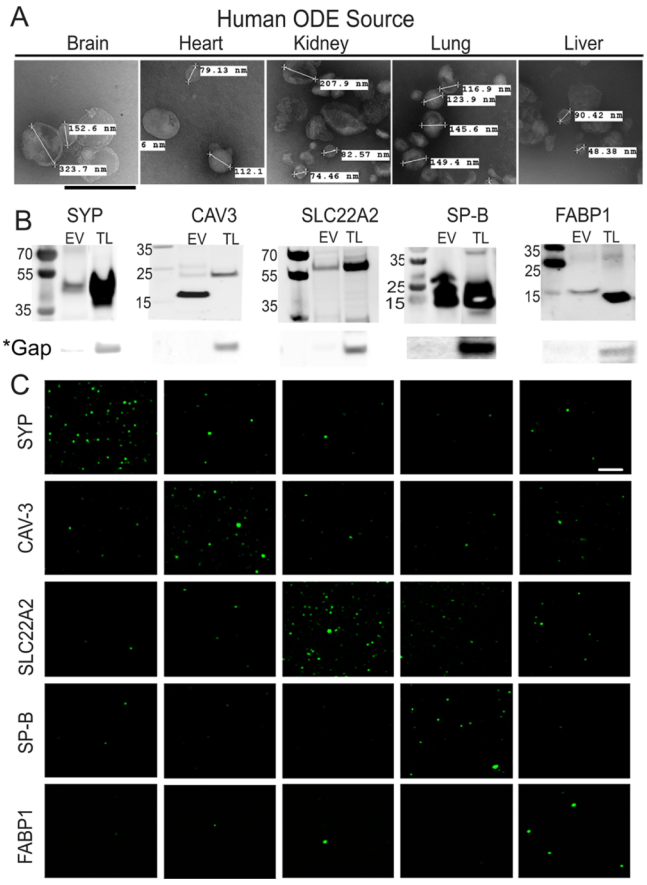

Figure 8. Human ODEs. (A) TEM analyses of human-derived ODE, original scale bar, 500 nm (B) Immunoblotting on select tissue markers and Gapdh (*Gap) was used as a cytoplasmic marker control. (C) Human ODEs from five organs were immunolabeled for organ-specific surface markers. Imaging confirmed high selectivity of these markers among different organ types. Scale bar, 20 μm.

compared to EV proteins isolated from rat organs even when similar weights of the starting material were used (Table S5). This discrepancy could be attributed to the time elapsed between death and collection of tissues (postmortem interval) that could invariably result in loss of protein integrity that could lead to denaturation of tissue proteins. Interestingly, EVs derived from human lung showed no bud membrane protrusions as seen for rat lung-derived EVs (Figure S6). The size range of these vesicles ranged between 50 and 300 nm. Next, we performed molecular analyses on select protein markers. Immunoblotting showed that ODE samples were positive for EV-specific protein markers (Hsp-70, CD63, CD81), whereas the negative marker (calnexin) was present only in the whole tissue lysates (Figure S8). Both ODE and tissue samples also showed the presence of tissue markers identified from our rat study (Figure 8B): SYP (brain), CAV3 (heart), SLC22A2 (kidney), SP-B (lung), and FABP1 (liver). Single EV imaging further confirmed the tissue-specific nature of these markers (Figure 8C); the number of marker-positive vesicles was the highest only when tissue-type was matched. Because total EV concentrations varied among ODE sources, we normalized each column to the maximum EV numbers detected. The number of marker-positive EVs were counted, and heatmap was generated as shown in Figure S9. In summary, both rat and human ODE show similar EV marker expression profiles, thus denoting their respective use as potential markers in both preclinical and clinical applications.

CONCLUSIONS

Using both biochemical and single-EV imaging methods, we show a proof of concept for identifying specific EV markers for brain, lung, heart, kidney, and liver using both preclinical (rat) and clinical (human) model systems. ODE can cross tissue barriers and circulate in blood, thereby serving as a promising noninvasive biomarker to detect organ dysfunctions. Our proteomic analysis of ODE revealed that the protein signatures identified from different organs are distinct from one another. Upon postvalidation by western blot and single EV imaging on both rat and human ODE, we confirmed SYP, CAV3, SLC22A2, SP-B, and FABP1 as specific markers for the brain, heart, kidney, lung, and liver, respectively.

Although we validated one marker for each organ, there is a strong possibility of more potential organ-specific markers in

https://dx.doi.org/10.1021/acsanm.0c01654
ACS Appl. Nano Mater. 2020, 3, 8906−8919

Table 1. Details for Primary and Secondary Antibodies Used for Western Blot Analysis

marker	running condition	antibody (catalog #)	sample species	1° Ab dilution	2° Ab dilution
Hsp-70	reducing	SAB4200714	rat/human	1:1000	1:2000
flotillin-1	reducing	abcam41927	rat/human	1:1000	1:2000
calnexin	reducing	ab22595	rat/human	1:1000	1:2000
SYP	reducing	PA1-1043	rat/human	1:1000	1:2000
CAV3	reducing	ab2912	rat	1:1000	1:2000
CAV3	reducing	MAB6706	human	1:1000	1:2000
SLC22A2	reducing	PA5-37290	rat	1:500	1:1000
SLC22A2	reducing	MAB6547	human	1:500	1:1000
ANXA5	reducing	ab14196	rat	1:500	1:2000
FABP1	reducing	Invitrogen 720242	rat/human	1:500	1:1000
COX5B	reducing	ab180136	rat	1:10,000	1:20,000
ICAM-1	reducing	sc-107	rat	1:500	1:1000
MOG	reducing	MA5-24645	rat	1:500	1:1000
SLC12A1	reducing	ab171747	rat	1:1000	1:2000
NCAM1	reducing	ab232781	rat	1:500	1:1000
MGST1	reducing	ab129175	rat	1:500	1:1000
GSTM1	reducing	ab108524	rat	1:1000	1:2000
EAAT1	reducing	sc-515839	rat	1:1000	1:2000
HSD3B7	reducing	ab190223	rat	1:500	1:1000
CHIA	reducing	PA5-03057	rat	1:1000	1:2000
SP-B	non-reducing	WRAB-48604	rat/human	1:1000	1:2000
CD81	non-reducing	MCA1846	rat	1:500	1:1000
CD81	non-reducing	MAB4615	human	1:500	1:1000
CD63	non-reducing	BD551458	rat/human	1:500	1:1000

ODEs. Therefore, more stringent strategies such as tandem or sequential immunoprecipitation might be required to pull down organ-specific EVs. A more thorough analysis of the data needs to be performed to ascertain the cellular origin of EVs. Therefore, we recommend using more than one EV protein marker for organ-specific screening. In summary, our robust approach provides a valuable proof-of-concept approach in defining specific ODE markers, which further could be developed as potential therapeutic candidates for respective end organ-associated pathologies.

MATERIALS AND METHODS

Animals. Male and female Sprague Dawley rats were obtained from Charles River Laboratories Inc. (Wilmington, MA, USA) and group-housed in a 12 h light−dark cycle and fed *ad libitum*. All procedures and protocols were approved by the Institutional Animal Care and Use Committee of the University of Nebraska Medical Center and conducted in accordance with the National Institutes of Health Guide for the Care and Use of Laboratory Animals.

Isolation of Organs. We employed both perfusion and nonperfusion methods to isolate the brain, heart, kidney, lung, and liver from the animals. For isolation employing perfusion, animals were deeply anesthetized using isoflurane followed by infusion with 1× phosphate-buffered saline (PBS; 70013-032, Gibco-Thermo Fisher Scientific, Waltham, MA, USA) using a peristaltic pump (Fisherbrand variable-flow peristaltic pump, Waltham, MA, USA) to clear the blood. Animals that did not undergo perfusions were sacrificed via overdose of isoflurane followed by decapitation and retrieval of organs. The different organs were harvested and immediately flash-frozen on dry ice, followed by storage at −80 °C until further use.

Human Organs. Human postmortem tissues (heart, lung, liver, and kidney) from two donors were obtained from the National Disease Research Interchange (NDRI) (Philadelphia, PA, USA), and human postmortem brain samples from two additional donors were obtained from the UCLA National Neurological AIDS Bank of the National NeuroAIDS Tissue Consortium (NNTC). All samples were stored at −80 °C until further use. See Table S3 for additional information on donors.

EV Isolations. EV isolations were carried out as described in our previous studies with minor modifications.[31,32,78] This protocol is well-verified, and we have consistently got similar results in all the runs that were performed for this study. In brief, tissues weighing ∼450 mg (Table S4) each were minced and treated with 20 unit/mL papain (P4762, Sigma-Aldrich, MO, USA) in 3.5 mL of Hibernate A (NC0176976, Fisher Scientific, Hampton, NH, USA) solution and rocked for 15−25 min (brain, 15 min; kidney and liver, 20 min; heart and lung, 25 min) at 37 °C. The reaction was then quenched with 6.5 mL of cold Hibernate A solution and gently homogenized using a glass pipette. Tissue homogenate was sequentially centrifuged at 300*g* for 10 min, 2000*g* for 10 min, and at 10,000*g* for 30 min at 4 °C to remove dead cells, cell debris, and larger vesicles, respectively. The supernatant was then filtered through a 0.20 μm syringe filter (09-754-13, Corning Fisher Scientific, Hampton, NH, USA) and centrifuged at 100,000*g* for 70 min at 4 °C to pellet down the EVs. The EV pellet was then resuspended in 37 mL particle-free cold 1× PBS and centrifuged again at 100,000*g* for 70 min at 4 °C. A sucrose gradient was prepared using 2 mL steps starting from 2.0 M sucrose at the bottom with a 0.25 M sucrose solution at the top. The washed EV pellet was resuspended in 2 mL of 0.95 M sucrose solution and layered between 0.60 and 1.30 M sucrose layers. The gradients were then centrifuged at 200,000 for 16 h at 4 °C. To make sure layers should not mix, we used lower acceleration (7) and lower deceleration (7) during our overnight run. After the run was complete, we immediately removed respective layers. For collecting the purified EVs, a 2 mL fraction was discarded from the top of the gradient, and the next 8 mL of the gradient was collected, diluted to 37 mL with cold particle-free PBS, and centrifuged at 100,000*g* at 4 °C for 70 min. EV pellets were suspended in 50−100 μL of particle-free PBS and further used for downstream analysis.

Nanoparticle Tracking Analysis. EV size distribution curves and concentration measurements were carried out by NTA using a Nanosight NS300TM (Malvern Instruments, UK). For NTA analysis, EV pellets were resuspended in 100 μL of PBS, following which 10 μL of the sample was diluted to 1:100 to 1:1000 in PBS prior to measurements. All samples were loaded with the laser module outside

https://dx.doi.org/10.1021/acsanm.0c01654
ACS Appl. Nano Mater. 2020, 3, 8906−8919

Table 2. Details for Primary and Secondary Antibodies Used for SEA

marker	antibody (catalog #)	sample species	1° Ab dilution	2° Ab dilution
SYP	PA1-1043	rat/human	1:100/1:50	1:500/1:200
CAV3	ab2912	rat	1:100	1:500
CAV3	MAB6706	human	1:50	1:400
SLC22A2	PA5-37290	rat	1:100	1:500
SLC22A2	MAB6547	human	1:50	1:400
ANXA5	ab14196	rat	1:100	1:500
SP-B	WRAB-48604	human	1:50	1:100
FABP1	CST 13368	rat/human	1:50/1:50	1:200/1:100

the instrument. As the sample was loaded, care was taken to avoid air pockets. The machine was equipped with a 488 nm laser and a syringe pump system, with a pump infusion speed of 20. The standard measurement option was selected for the scripted workflow to capture videos. The number and duration of captures were set to 5 and 60 s, respectively. The base filename and location were selected prior to starting the run. The camera level was set at 11. Background measurements were performed with filtered PBS, which revealed the absence of any kind of particles. Five video recordings were carried out for each EV preparation with a duration of 60 s with frame rates of 25 frames/s. Once the videos were recorded, the NTA 3.1 software version was used to analyze the sample videos. For analysis, the screen gain was set to 1.0, and the detection threshold was adjusted to set the minimum brightness of pixels to be considered. At the end of the analyses, the dilution factor for the samples was updated before data export.

Transmission Electron Microscopy. For TEM, a 10 μL EV sample was mixed with 90 μL of TEM fix buffer (2% glutaraldehyde, 2% paraformaldehyde, and 0.1 M phosphate buffer). A 10 μL drop of EV-buffer mix sample was spotted onto formvar-/silicon monoxide-coated 200 mesh copper grids (Ted Pella Inc. Redding, CA) and allowed to sit for 3 min. Grids were glow-discharged for 60 s at 20 μA using a GloQube glow discharge unit (Quorum Technologies, East Sussex, UK) prior to use. The excess solution was blotted off by using a clean piece of Whatman #50 filter paper held by forceps at a 45° angle to touch only the edge of the grid, leaving behind a thin film of the sample that was allowed to dry for 1 min. Samples were negatively stained with NanoVan (Nanoprobes, New York, NY) and examined on a Tecnai G^2 Spirit TWIN (FEI, Hillsboro, OR) operating at an accelerating voltage of 80 kV. Images were acquired digitally with an AMT (Woburn, MA) digital imaging system.

Western Blotting. EV pellets were homogenized in radioimmunoprecipitation assay (RIPA) buffer containing 1% sodium dodecyl sulfate (SDS), and protein-estimated using the bicinchoninic acid protein assay kit (Thermo Fisher Scientific, Rockford, IL, USA). Western blotting was performed on the various tissue-specific EVs as described previously.[31,78,79] In brief, 20−40 μg of the protein was loaded onto NuPAGE 4−12% bis−Tris gels (Invitrogen) and run either under nonreducing (CD63 and CD81) or reducing (Hsp-70 and flotillin-1) conditions followed by their transfer onto nitrocellulose membranes using the iBlot 2 gel transfer device (Invitrogen). Membranes were blocked in TBS SuperBlock buffer (Thermo Fisher Scientific) for 30 min, and immunoblotting was carried out overnight at 4 °C with primary antibodies (see Table 1 for details). The next day, membranes were incubated with respective horseradish peroxidase-conjugated secondary antibodies for 1.5 h at room temperature on a rocker. Blots were developed with 1:1 solution of Radiance chemiluminescent substrate and luminol/enhancer (Azure Biosystems) and visualized using a c300 imaging system (Azure Biosystems). Images were quantified using the ImageJ software.

Proteomics. A total of 100 μg of the EV protein was prepared using RIPA buffer with 1% SDS per sample from three biological replicates, and the detergent was removed by chloroform/methanol extraction. Samples were then subjected to quantitative mass spectrometry-based proteomics. In brief, the protein pellet was resuspended in 100 mM ammonium bicarbonate and digested with MS-grade trypsin (Pierce) overnight at 37 °C. Peptides cleaned with PepClean C18 spin columns (Thermo Fisher Scientific) were resuspended in 2% acetonitrile (ACN) and 0.1% formic acid (FA). A total of 500 ng from each sample was loaded onto the trap column of Acclaim PepMap 100 75 μm × 2 cm C18 LC Columns (Thermo Fisher Scientific) at a flow rate of 4 μL/min. Subsequently, samples were separated using a Thermo RSLC Ultimate 3000 (Thermo Fisher Scientific) on a Thermo EASY-Spray PepMap RSLC C18 75 μm × 50 cm C-18 2 μm column (Thermo Fisher Scientific, Waltham, MA, USA) with a step gradient of 4−25% solvent B (0.1% FA in 80% ACN) from 10 to 130 min and 25−45% solvent B for 130−145 min at 300 nL/min and 50 °C with a 180 min total run time. Thermo Orbitrap Fusion Lumos Tribrid (Thermo Fisher Scientific) mass spectrometer (data-dependent acquisition mode) was used to analyze the eluted peptides. By Orbitrap, with a resolution of 120,000, the full survey scan MS (from m/z 350−1800) was acquired. The ion filling time was set as 100 ms, while the automatic gain control (AGC) target for MS was set as 4×10^5. The precursor ions with charge state 2−6 were isolated in a 3 s cycle and fragmented using higher energy collisional dissociation (HCD) fragmentation with 35% normalized collision energy and were detected at a mass resolution of 30,000 at 200 m/z. For tandem mass spectrometry (MS/MS), the AGC target was set as $5 \times 10^{4,}$ and ion filling time was set as 60 ms, while dynamic separation was set for 30 s with a 10 ppm mass window. The protein identification was performed by searching MS/MS data against the Swiss-Prot *Rattus norvegicus* protein database downloaded on Feb 13, 2019, using the in-house mascot 2.6.2 (Matrix Science) search engine. With a maximum of two unexploited cleavage sites, the search was set up for full tryptic peptides. N-Terminus acetylation and oxidized methionine were included as variable modifications, whereas cysteine carbamidomethylation was set as a fixed modification. Forerunner mass tolerance threshold was set at 10 ppm, and the maximum fragment mass error was 0.02 Da. The significance threshold score of the ion was calculated based on a FDR (calculated using false-positive matches/true positive matches + false-positive matches) of ≤1% (http://www.matrixscience.com/help/decoy_help.html). Qualitative analysis was performed using progenesis QI proteomics 4.1 (Nonlinear dynamics). Sample-to-sample experimental variation during sample runs was normalized using default settings (normalize to all proteins) in progenesis QI proteomics.

Data Analysis and Bioinformatics. Proteins identified with at least two unique peptides were included in the downstream differential analysis. Proteins were further filtered from downstream analysis if the spectral counts were missing in 80% of the samples, irrespective of the sample type. Spectral counts were analyzed using limma[80] to identify differentially expressed proteins between any two EV types. A total of 10 pairwise differential expression analyses were performed across all sample groups based on the tissue of origin. A protein was identified to be differentially expressed if the FDR (Benjamini and Hochberg's method) corrected P-value was ≤0.05, and log 2-fold change was ≥1.5. A heatmap of the top 25 proteins in each organ that exhibited significantly higher or lower expression with respect to other comparisons was plotted using the function heatmap.2 in the R (version 3.6.0) package gplots. PCA was performed using ClustVis.[81] Gene ontology (GO) analysis of differentially expressed proteins was performed using the Cytoscape plugin ClueGO.[82] Only proteins exhibiting significantly higher expression across all comparisons were included in this analysis.

https://dx.doi.org/10.1021/acsanm.0c01654
ACS Appl. Nano Mater. 2020, 3, 8906−8919

The biological process, molecular function, and Kyoto Encyclopedia of Genes and Genome pathways were included for GO enrichment analysis.

SEA for Organ-Specific Protein Markers. EVs from different organ tissues were prepared as described above. EV pellets were suspended in PBS and then filtered with a 0.22 μm syringe filter (SLGVR04NL, Millipore Sigma). Filtered EVs were captured on a glass slide. Following 30 min incubation (20 °C), the slide was washed with PBS buffer containing 0.001% Tween 20 (PBST). After incubation with the fixation buffer (4% formaldehyde), permiabilization buffer (BD perm/wash buffer, 554723, BD Biosciences), and blocking buffer (SuperBlock, 37515, Thermo Scientific), EV samples were incubated with primary antibodies (see Table 2 for antibody details). After washing with PBST, the fluorescence-conjugated secondary antibody was incubated for 30 min (20 °C) and washed again. Fluorescence images were taken with an upright fluorescent microscope (BX63, Olympus) using a 40× objective lens. Acquisition settings (i.e., magnification, exposure time, camera gains, illumination) were kept constant for all images.

■ ASSOCIATED CONTENT

Supporting Information

The Supporting Information is available free of charge at https://pubs.acs.org/doi/10.1021/acsanm.0c01654.

Total EV protein yield from nonperfused and perfused rat tissues (PDF)

Differentially expressed proteins in the brain, heart, kidney, lung, and liver (XLSX)

Spectral counts of abundant proteins from the EV of rat brain, heart, kidney, lung, and liver (XLSX)

Additional information on human donors (XLSX)

EV protein yields for different human organs (PDF)

TEM analysis of EV isolated from perfused rat organs, western blot analysis of EVs purified from perfused rat organs, bar charts representing the enriched GO annotations, characterization of organ-specific EV protein markers; brain, heart, kidney, lung, and liver, comparative expression of L1CAM and SYP in rat EV, single EV imaging for ODEs with five organ-specific markers, TEM and NTA analysis of EVs isolated from postmortem human organs, western blot analysis of human EVs and human tissue lysates, signal contrast among human ODE types and organ-specific markers (PDF)

■ AUTHOR INFORMATION

Corresponding Author

Sowmya V. Yelamanchili − *Department of Anesthesiology, University of Nebraska Medical Center, Omaha, Nebraska 68198, United States;* orcid.org/0000-0003-1530-0527; Phone: 402-559-5348; Email: syelamanchili@unmc.edu

Authors

Subhash Chand − *Department of Anesthesiology, University of Nebraska Medical Center, Omaha, Nebraska 68198, United States*

Ala Jo − *Center for Systems Biology and Department of Radiology, Massachusetts General Hospital, Boston, Massachusetts 02114, United States*

Neetha Nanoth Vellichirammal − *Department of Genetics, Cell Biology and Anatomy, University of Nebraska Medical Center, Omaha, Nebraska 68198, United States*

Austin Gowen − *Department of Anesthesiology, University of Nebraska Medical Center, Omaha, Nebraska 68198, United States*

Chittibabu Guda − *Department of Genetics, Cell Biology and Anatomy, University of Nebraska Medical Center, Omaha, Nebraska 68198, United States*

Victoria Schaal − *Department of Anesthesiology, University of Nebraska Medical Center, Omaha, Nebraska 68198, United States*

Katherine Odegaard − *Department of Anesthesiology, University of Nebraska Medical Center, Omaha, Nebraska 68198, United States*

Hakho Lee − *Center for Systems Biology and Department of Radiology, Massachusetts General Hospital, Boston, Massachusetts 02114, United States;* orcid.org/0000-0002-0087-0909

Gurudutt Pendyala − *Department of Anesthesiology, University of Nebraska Medical Center, Omaha, Nebraska 68198, United States*

Complete contact information is available at: https://pubs.acs.org/10.1021/acsanm.0c01654

Author Contributions

The manuscript was written through contributions of all authors. All authors have given approval to the final version of the manuscript.

Funding

This study is supported by NIDA grants R21DA046855 and R01DA042379 awarded to S.V.Y., R21DA049577 to G.P. and H.L. and R01DA046852 to G.P. and S.V.Y. The bioinformatics work has been partially supported by the National Institutes of Health grants to C.G. [5P20GM103427, 1P30GM127200].

Notes

The authors declare the following competing financial interest(s): The authors have filed intellectual property for organ specific EV markers that were identified in this study. The proteomics data have been deposited to the ProteomeXchange Consortium via the PRIDE partner repository with the data set identifier PXD020568.

■ ACKNOWLEDGMENTS

We thank the University of Nebraska Medical Center Mass Spectrometry and Proteomics Core Facility for its expert assistance. The UNMC Mass Spectrometry and Proteomics Core Facility is administrated through the Office of the Vice Chancellor for Research and supported by state funds from the Nebraska Research Initiative (NRI). We also thank Tom Bargar and Nicholas Conoan for their expert technical assistance for TEM.

■ REFERENCES

(1) Porro, C.; Trotta, T.; Panaro, M. A. Microvesicles in the brain: Biomarker, messenger or mediator? *J. Neuroimmunol.* **2015**, *288*, 70−78.

(2) Mathieu, M.; Martin-Jaular, L.; Lavieu, G.; Théry, C. Specificities of secretion and uptake of exosomes and other extracellular vesicles for cell-to-cell communication. *Nat. Cell Biol.* **2019**, *21*, 9−17.

(3) Antonyak, M. A.; Cerione, R. A. Emerging picture of the distinct traits and functions of microvesicles and exosomes. *Proc. Natl. Acad. Sci. U.S.A.* **2015**, *112*, 3589−3590.

(4) Maas, S. L. N.; Breakefield, X. O.; Weaver, A. M. Extracellular Vesicles: Unique Intercellular Delivery Vehicles. *Trends Cell Biol.* **2017**, *27*, 172−188.

(5) Raposo, G.; Stoorvogel, W. Extracellular vesicles: exosomes, microvesicles, and friends. *J. Cell Biol.* **2013**, *200*, 373−383.
(6) Valadi, H.; Ekström, K.; Bossios, A.; Sjöstrand, M.; Lee, J. J.; Lötvall, J. O. Exosome-mediated transfer of mRNAs and microRNAs is a novel mechanism of genetic exchange between cells. *Nat. Cell Biol.* **2007**, *9*, 654.
(7) Chen, R.; Xu, X.; Qian, Z.; Zhang, C.; Niu, Y.; Wang, Z.; Sun, J.; Zhang, X.; Yu, Y. The biological functions and clinical applications of exosomes in lung cancer. *Cell. Mol. Life Sci.* **2019**, *76*, 4613.
(8) Shah, R.; Patel, T.; Freedman, J. E. Circulating Extracellular Vesicles in Human Disease. *N. Engl. J. Med.* **2018**, *379*, 958−966.
(9) Jiang, L.; Gu, Y.; Du, Y.; Liu, J. Exosomes: Diagnostic Biomarkers and Therapeutic Delivery Vehicles for Cancer. *Mol. Pharm.* **2019**, *16*, 3333−3349.
(10) Wu, M.; Wang, G.; Hu, W.; Yao, Y.; Yu, X. F. Emerging roles and therapeutic value of exosomes in cancer metastasis. *Mol. Cancer* **2019**, *18*, 53.
(11) Hosaka, T.; Yamashita, T.; Tamaoka, A.; Kwak, S. Extracellular RNAs as Biomarkers of Sporadic Amyotrophic Lateral Sclerosis and Other Neurodegenerative Diseases. *Int. J. Mol. Sci.* **2019**, *20*, 3148.
(12) Rodrigues, M.; Richards, N.; Ning, B.; Lyon, C. J.; Hu, T. Y. Rapid Lipid-Based Approach for Normalization of Quantum-Dot-Detected Biomarker Expression on Extracellular Vesicles in Complex Biological Samples. *Nano Lett.* **2019**, *19*, 7623.
(13) Morales-Kastresana, A.; Musich, T. A.; Welsh, J. A.; Telford, W.; Demberg, T.; Wood, J. C. S.; Bigos, M.; Ross, C. D.; Kachynski, A.; Dean, A.; Felton, E. J.; Van Dyke, J.; Tigges, J.; Toxavidis, V.; Parks, D. R.; Overton, W. R.; Kesarwala, A. H.; Freeman, G. J.; Rosner, A.; Perfetto, S. P.; Pasquet, L.; Terabe, M.; McKinnon, K.; Kapoor, V.; Trepel, J. B.; Puri, A.; Kobayashi, H.; Yung, B.; Chen, X.; Guion, P.; Choyke, P.; Knox, S. J.; Ghiran, I.; Robert-Guroff, M.; Berzofsky, J. A.; Jones, J. C. High-fidelity detection and sorting of nanoscale vesicles in viral disease and cancer. *J. Extracell. Vesicles* **2019**, *8*, 1597603.
(14) Zhang, P.; Zhou, X.; Zeng, Y. Multiplexed immunophenotyping of circulating exosomes on nano-engineered ExoProfile chip towards early diagnosis of cancer. *Chem. Sci.* **2019**, *10*, 5495−5504.
(15) Shahjin, F.; Chand, S.; Yelamanchili, S. V. Extracellular Vesicles as Drug Delivery Vehicles to the Central Nervous System. *J. Neuroimmune Pharmacol.* **2019**, 1.
(16) Kanninen, K. M.; Bister, N.; Koistinaho, J.; Malm, T. Exosomes as new diagnostic tools in CNS diseases. *Biochim. Biophys. Acta* **2016**, *1862*, 403−410.
(17) Pulliam, L.; Sun, B.; Mustapic, M.; Chawla, S.; Kapogiannis, D. Plasma neuronal exosomes serve as biomarkers of cognitive impairment in HIV infection and Alzheimer's disease. *J. NeuroVirol.* **2019**, *25*, 702.
(18) Tang, Y.; Zhao, S.; Wang, J.; Li, D.; Ren, Q.; Tang, Y. Plasma miR-122 as a potential diagnostic and prognostic indicator in human glioma. *Neurol. Sci.* **2017**, *38*, 1087−1092.
(19) Shao, N.; Wang, L.; Xue, L.; Wang, R.; Lan, Q. Plasma miR-454-3p as a potential prognostic indicator in human glioma. *Neurol. Sci.* **2015**, *36*, 309−313.
(20) Lan, F.; Qing, Q.; Pan, Q.; Hu, M.; Yu, H.; Yue, X. Serum exosomal miR-301a as a potential diagnostic and prognostic biomarker for human glioma. *Cell. Oncol.* **2018**, *41*, 25−33.
(21) Yue, X.; Lan, F.; Hu, M.; Pan, Q.; Wang, Q.; Wang, J. Downregulation of serum microRNA-205 as a potential diagnostic and prognostic biomarker for human glioma. *J. Neurosurg.* **2016**, *124*, 122−128.
(22) Shi, R.; Wang, P.-Y.; Li, X.-Y.; Chen, J.-X.; Li, Y.; Zhang, X.-Z.; Zhang, C.-G.; Jiang, T.; Li, W.-B.; Ding, W.; Cheng, S.-J. Exosomal levels of miRNA-21 from cerebrospinal fluids associated with poor prognosis and tumor recurrence of glioma patients. *Oncotarget* **2015**, *6*, 26971−26981.
(23) Li, M.; Zeringer, E.; Barta, T.; Schageman, J.; Cheng, A.; Vlassov, A. V. Analysis of the RNA content of the exosomes derived from blood serum and urine and its potential as biomarkers. *Philos. Trans. R. Soc., B* **2014**, *369*, 20130502.
(24) Wong, C.-H.; Chen, Y.-C. Clinical significance of exosomes as potential biomarkers in cancer. *World J. Clin. Cases* **2019**, *7*, 171−190.
(25) Vlassov, A. V.; Magdaleno, S.; Setterquist, R.; Conrad, R. Exosomes: current knowledge of their composition, biological functions, and diagnostic and therapeutic potentials. *Biochim. Biophys. Acta* **2012**, *1820*, 940−948.
(26) Revenfeld, A. L. S.; Bæk, R.; Nielsen, M. H.; Stensballe, A.; Varming, K.; Jørgensen, M. Diagnostic and prognostic potential of extracellular vesicles in peripheral blood. *Clin. Ther.* **2014**, *36*, 830−846.
(27) Jansen, F.; Nickenig, G.; Werner, N. Extracellular Vesicles in Cardiovascular Disease. *Circ. Res.* **2017**, *120*, 1649−1657.
(28) Crescitelli, R.; Lässer, C.; Jang, S. C.; Cvjetkovic, A.; Malmhäll, C.; Karimi, N.; Höög, J. L.; Johansson, I.; Fuchs, J.; Thorsell, A.; Gho, Y. S.; Olofsson Bagge, R.; Lötvall, J. Subpopulations of extracellular vesicles from human metastatic melanoma tissue identified by quantitative proteomics after optimized isolation. *J. Extracell. Vesicles* **2020**, *9*, 1722433.
(29) Ishiguro, K.; Yan, I. K.; Patel, T. Isolation of Tissue Extracellular Vesicles from the Liver. *J. Visualized Exp.* **2019**, No. e58649.
(30) Vella, L. J.; Scicluna, B. J.; Cheng, L.; Bawden, E. G.; Masters, C. L.; Ang, C.-S.; Willamson, N.; McLean, C.; Barnham, K. J.; Hill, A. F. A rigorous method to enrich for exosomes from brain tissue. *J. Extracell. Vesicles* **2017**, *6*, 1348885.
(31) Yelamanchili, S. V.; Lamberty, B. G.; Rennard, D. A.; Morsey, B. M.; Hochfelder, C. G.; Meays, B. M.; Levy, E.; Fox, H. S. MiR-21 in Extracellular Vesicles Leads to Neurotoxicity via TLR7 Signaling in SIV Neurological Disease. *PLoS Pathog.* **2015**, *11*, No. e1005032.
(32) Perez-Gonzalez, R.; Gauthier, S. A.; Kumar, A.; Levy, E. The exosome secretory pathway transports amyloid precursor protein carboxyl-terminal fragments from the cell into the brain extracellular space. *J. Biol. Chem.* **2012**, *287*, 43108−43115.
(33) Harrison, E. B.; Hochfelder, C. G.; Lamberty, B. G.; Meays, B. M.; Morsey, B. M.; Kelso, M. L.; Fox, H. S.; Yelamanchili, S. V. Traumatic brain injury increases levels of miR-21 in extracellular vesicles: implications for neuroinflammation. *FEBS Open Bio* **2016**, *6*, 835−846.
(34) Kowal, J.; Arras, G.; Colombo, M.; Jouve, M.; Morath, J. P.; Primdal-Bengtson, B.; Dingli, F.; Loew, D.; Tkach, M.; Théry, C. Proteomic comparison defines novel markers to characterize heterogeneous populations of extracellular vesicle subtypes. *Proc. Natl. Acad. Sci. U.S.A.* **2016**, *113*, E968−E977.
(35) Huang, Y.; Cheng, L.; Turchinovich, A.; Mahairaki, V.; Troncoso, J. C.; Pletniková, O.; Haughey, N. J.; Vella, L. J.; Hill, A. F.; Zheng, L.; Witwer, K. W. Influence of species and processing parameters on recovery and content of brain tissue-derived extracellular vesicles. *J. Extracell. Vesicles* **2020**, *9*, 1785746.
(36) Vagner, T.; Chin, A.; Mariscal, J.; Bannykh, S.; Engman, D. M.; Di Vizio, D. Protein Composition Reflects Extracellular Vesicle Heterogeneity. *Proteomics* **2019**, *19*, 1800167.
(37) Jalalian, S. H.; Ramezani, M.; Jalalian, S. A.; Abnous, K.; Taghdisi, S. M. Exosomes, new biomarkers in early cancer detection. *Anal. Biochem.* **2019**, *571*, 1−13.
(38) Saenz-Pipaon, G.; San Martín, P.; Planell, N.; Maillo, A.; Ravassa, S.; Vilas-Zornoza, A.; Martinez-Aguilar, E.; Rodriguez, J. A.; Alameda, D.; Lara-Astiaso, D.; Prosper, F.; Paramo, J. A.; Orbe, J.; Gomez-Cabrero, D.; Roncal, C. Functional and transcriptomic analysis of extracellular vesicles identifies calprotectin as a new prognostic marker in peripheral arterial disease (PAD). *J. Extracell. Vesicles* **2020**, *9*, 1729646.
(39) Saeedi, S.; Israel, S.; Nagy, C.; Turecki, G. The emerging role of exosomes in mental disorders. *Transl. Psychiatry* **2019**, *9*, 122.
(40) Fiandaca, M. S.; Kapogiannis, D.; Mapstone, M.; Boxer, A.; Eitan, E.; Schwartz, J. B.; Abner, E. L.; Petersen, R. C.; Federoff, H. J.; Miller, B. L.; Goetzl, E. J. Identification of preclinical Alzheimer's disease by a profile of pathogenic proteins in neurally derived blood exosomes: A case-control study. *Alzheimers. Dement* **2015**, *11*, 600−607.e1.

https://dx.doi.org/10.1021/acsanm.0c01654
ACS Appl. Nano Mater. 2020, 3, 8906−8919

(41) Pulliam, L.; Sun, B.; Mustapic, M.; Chawla, S.; Kapogiannis, D. Plasma neuronal exosomes serve as biomarkers of cognitive impairment in HIV infection and Alzheimer's disease. *J. NeuroVirol.* **2019**, *25*, 702−709.
(42) Dagur, R. S.; Liao, K.; Sil, S.; Niu, F.; Sun, Z.; Lyubchenko, Y. L.; Peeples, E. S.; Hu, G.; Buch, S. Neuronal-derived extracellular vesicles are enriched in the brain and serum of HIV-1 transgenic rats. *J. Extracell. Vesicles* **2020**, *9*, 1703249.
(43) Dagur, R. S.; Liao, K.; Sil, S.; Niu, F.; Sun, Z.; Lyubchenko, Y. L.; Peeples, E. S.; Hu, G.; Buch, S. Neuronal-derived extracellular vesicles are enriched in the brain and serum of HIV-1 transgenic rats. *J. Extracell. Vesicles* **2020**, *9*, 1703249.
(44) Sun, B.; Dalvi, P.; Abadjian, L.; Tang, N.; Pulliam, L. Blood neuron-derived exosomes as biomarkers of cognitive impairment in HIV. *AIDS* **2017**, *31*, F9−f17.
(45) Südhof, T. C.; Jahn, R. Proteins of synaptic vesicles involved in exocytosis and membrane recycling. *Neuron* **1991**, *6*, 665−677.
(46) Goetzl, E. J.; Kapogiannis, D.; Schwartz, J. B.; Lobach, I. V.; Goetzl, L.; Abner, E. L.; Jicha, G. A.; Karydas, A. M.; Boxer, A.; Miller, B. L. Decreased synaptic proteins in neuronal exosomes of frontotemporal dementia and Alzheimer's disease. *FASEB J.* **2016**, *30*, 4141−4148.
(47) Agliardi, C.; Guerini, F. R.; Zanzottera, M.; Bianchi, A.; Nemni, R.; Clerici, M. SNAP-25 in Serum Is Carried by Exosomes of Neuronal Origin and Is a Potential Biomarker of Alzheimer's Disease. *Mol. Neurobiol.* **2019**, *56*, 5792−5798.
(48) Winston, C. N.; Romero, H. K.; Ellisman, M.; Nauss, S.; Julovich, D. A.; Conger, T.; Hall, J. R.; Campana, W.; O'Bryant, S. E.; Nievergelt, C. M.; Baker, D. G.; Risbrough, V. B.; Rissman, R. A. Assessing Neuronal and Astrocyte Derived Exosomes From Individuals With Mild Traumatic Brain Injury for Markers of Neurodegeneration and Cytotoxic Activity. *Front. Neurosci.* **2019**, *13*, 1005.
(49) Cohen, A. W.; Hnasko, R.; Schubert, W.; Lisanti, M. P. Role of caveolae and caveolins in health and disease. *Physiol. Rev.* **2004**, *84*, 1341−1379.
(50) Waldenström, A.; Gennebäck, N.; Hellman, U.; Ronquist, G. Cardiomyocyte microvesicles contain DNA/RNA and convey biological messages to target cells. *PLoS One* **2012**, *7*, No. e34653.
(51) Vallabhajosyula, P.; Korutla, L.; Habertheuer, A.; Yu, M.; Rostami, S.; Yuan, C.-X.; Reddy, S.; Liu, C.; Korutla, V.; Koeberlein, B.; Trofe-Clark, J.; Rickels, M. R.; Naji, A. Tissue-specific exosome biomarkers for noninvasively monitoring immunologic rejection of transplanted tissue. *J. Clin. Invest.* **2017**, *127*, 1375−1391.
(52) Habertheuer, A.; Korutla, L.; Rostami, S.; Reddy, S.; Lal, P.; Naji, A.; Vallabhajosyula, P. Donor tissue-specific exosome profiling enables noninvasive monitoring of acute rejection in mouse allogeneic heart transplantation. *J. Thorac. Cardiovasc. Surg.* **2018**, *155*, 2479−2489.
(53) Nigam, S. K. The SLC22 Transporter Family: A Paradigm for the Impact of Drug Transporters on Metabolic Pathways, Signaling, and Disease. *Annu. Rev. Pharmacol. Toxicol.* **2018**, *58*, 663−687.
(54) Urakami, Y.; Okuda, M.; Masuda, S.; Saito, H.; Inui, K. I. Functional characteristics and membrane localization of rat multispecific organic cation transporters, OCT1 and OCT2, mediating tubular secretion of cationic drugs. *J. Pharmacol. Exp. Ther.* **1998**, *287*, 800−805.
(55) Kimura, N.; Masuda, S.; Tanihara, Y.; Ueo, H.; Okuda, M.; Katsura, T.; Inui, K.-i. Metformin is a superior substrate for renal organic cation transporter OCT2 rather than hepatic OCT1. *Drug Metab. Pharmacokinet.* **2005**, *20*, 379−386.
(56) Yonezawa, A.; Masuda, S.; Nishihara, K.; Yano, I.; Katsura, T.; Inui, K.-i. Association between tubular toxicity of cisplatin and expression of organic cation transporter rOCT2 (Slc22a2) in the rat. *Biochem. Pharmacol.* **2005**, *70*, 1823−1831.
(57) Gonzales, P. A.; Pisitkun, T.; Hoffert, J. D.; Tchapyjnikov, D.; Star, R. A.; Kleta, R.; Wang, N. S.; Knepper, M. A. Large-scale proteomics and phosphoproteomics of urinary exosomes. *J. Am. Soc. Nephrol.* **2009**, *20*, 363−379.
(58) Console, L.; Scalise, M.; Indiveri, C. Exosomes in inflammation and role as biomarkers. *Clin. Chim. Acta* **2019**, *488*, 165−171.
(59) Amiri, A.; Pourhanifeh, M. H.; Mirzaei, H. R.; Nahand, J. S.; Moghoofei, M.; Sahebnasagh, R.; Mirzaei, H.; Hamblin, M. R. Exosomes and Lung cancer: Roles in pathophysiology, diagnosis and therapeutic applications. *Curr. Med. Chem.* **2020**, *27*, DOI: 10.2174/0929867327666200204141952.
(60) Sun, S.; Chen, H.; Xu, C.; Zhang, Y.; Zhang, Q.; Chen, L.; Ding, Q.; Deng, Z. Exosomal miR-106b serves as a novel marker for lung cancer and promotes cancer metastasis via targeting PTEN. *Life Sci.* **2020**, *244*, 117297.
(61) Niu, L.; Song, X.; Wang, N.; Xue, L.; Song, X.; Xie, L. Tumor-derived exosomal proteins as diagnostic biomarkers in non-small cell lung cancer. *Cancer Sci.* **2019**, *110*, 433−442.
(62) Sandfeld-Paulsen, B.; Jakobsen, K. R.; Bæk, R.; Folkersen, B. H.; Rasmussen, T. R.; Meldgaard, P.; Varming, K.; Jørgensen, M. M.; Sorensen, B. S. Exosomal Proteins as Diagnostic Biomarkers in Lung Cancer. *J. Thorac. Oncol.* **2016**, *11*, 1701−1710.
(63) Jacob, A.; Morley, M.; Hawkins, F.; McCauley, K. B.; Jean, J. C.; Heins, H.; Na, C.-L.; Weaver, T. E.; Vedaie, M.; Hurley, K.; Hinds, A.; Russo, S. J.; Kook, S.; Zacharias, W.; Ochs, M.; Traber, K.; Quinton, L. J.; Crane, A.; Davis, B. R.; White, F. V.; Wambach, J.; Whitsett, J. A.; Cole, F. S.; Morrisey, E. E.; Guttentag, S. H.; Beers, M. F.; Kotton, D. N. Differentiation of Human Pluripotent Stem Cells into Functional Lung Alveolar Epithelial Cells. *Cell Stem Cell* **2017**, *21*, 472−488 e10.
(64) Mannino, D. M. Biomarkers in COPD: the search continues! *Eur. Respir. J.* **2015**, *45*, 872−874.
(65) Sin, D. D.; Tammemagi, C. M.; Lam, S.; Barnett, M. J.; Duan, X.; Tam, A.; Auman, H.; Feng, Z.; Goodman, G. E.; Hanash, S.; Taguchi, A. Pro-surfactant protein B as a biomarker for lung cancer prediction. *J. Clin. Oncol.* **2013**, *31*, 4536−4543.
(66) Banfi, C.; Agostoni, P. Surfactant protein B: From biochemistry to its potential role as diagnostic and prognostic marker in heart failure. *Int. J. Cardiol.* **2016**, *221*, 456−462.
(67) Wang, G.; Bonkovsky, H. L.; de Lemos, A.; Burczynski, F. J. Recent insights into the biological functions of liver fatty acid binding protein 1. *J. Lipid Res.* **2015**, *56*, 2238−2247.
(68) Fu, S.; Wu, D.; Jiang, W.; Li, J.; Long, J.; Jia, C.; Zhou, T. Molecular Biomarkers in Drug-Induced Liver Injury: Challenges and Future Perspectives. *Front. Pharmacol.* **2020**, *10*, 1667.
(69) Lu, Y.-C.; Chang, C.-C.; Wang, C.-P.; Hung, W.-C.; Tsai, I.-T.; Tang, W.-H.; Wu, C.-C.; Wei, C.-T.; Chung, F.-M.; Lee, Y.-J.; Hsu, C.-C. Circulating fatty acid-binding protein 1 (FABP1) and nonalcoholic fatty liver disease in patients with type 2 diabetes mellitus. *Int. J. Med. Sci.* **2020**, *17*, 182−190.
(70) Jia, X.; Chen, J.; Megger, D. A.; Zhang, X.; Kozlowski, M.; Zhang, L.; Fang, Z.; Li, J.; Chu, Q.; Wu, M.; Li, Y.; Sitek, B.; Yuan, Z. Label-free Proteomic Analysis of Exosomes Derived from Inducible Hepatitis B Virus-Replicating HepAD38 Cell Line. *Mol. Cell. Proteomics* **2017**, *16*, S144−S160.
(71) Manner, A.; Islinger, M. Isolation of Peroxisomes from Rat Liver and Cultured Hepatoma Cells by Density Gradient Centrifugation. *Methods Mol. Biol.* **2017**, *1595*, 1−11.
(72) Darna, M.; Schmutz, I.; Richter, K.; Yelamanchili, S. V.; Pendyala, G.; Höltje, M.; Albrecht, U.; Ahnert-Hilger, G. Time of day-dependent sorting of the vesicular glutamate transporter to the plasma membrane. *J. Biol. Chem.* **2009**, *284*, 4300−4307.
(73) Reisinger, C.; Yelamanchili, S. V.; Hinz, B.; Mitter, D.; Becher, A.; Bigalke, H.; Ahnert-Hilger, G. The synaptophysin/synaptobrevin complex dissociates independently of neuroexocytosis. *J. Neurochem.* **2004**, *90*, 1−8.
(74) Mitter, D.; Reisinger, C.; Hinz, B.; Hollmann, S.; Yelamanchili, S. V.; Treiber-Held, S.; Ohm, T. G.; Herrmann, A.; Ahnert-Hilger, G. The synaptophysin/synaptobrevin interaction critically depends on the cholesterol content. *J. Neurochem.* **2003**, *84*, 35−42.
(75) Yelamanchili, S.; Reisinger, C.; Becher, A.; Sikorra, S.; Bigalke, H.; Binz, T.; Ahnert-Hilger, G. The C-terminal transmembrane region

https://dx.doi.org/10.1021/acsanm.0c01654
ACS Appl. Nano Mater. 2020, 3, 8906−8919

of synaptobrevin binds synaptophysin from adult synaptic vesicles. *Eur. J. Cell Biol.* **2005**, *84*, 467−475.
(76) Yelamanchili, S. V.; Pendyala, G.; Brunk, I.; Darna, M.; Albrecht, U.; Ahnert-Hilger, G. Differential sorting of the vesicular glutamate transporter 1 into a defined vesicular pool is regulated by light signaling involving the clock gene Period2. *J. Biol. Chem.* **2006**, *281*, 15671−15679.
(77) Lee, K.; Fraser, K.; Ghaddar, B.; Yang, K.; Kim, E.; Balaj, L.; Chiocca, E. A.; Breakefield, X. O.; Lee, H.; Weissleder, R. Multiplexed Profiling of Single Extracellular Vesicles. *ACS Nano* **2018**, *12*, 494−503.
(78) Moore, D.; Meays, B. M.; Madduri, L. S. V.; Shahjin, F.; Chand, S.; Niu, M.; Albahrani, A.; Guda, C.; Pendyala, G.; Fox, H. S.; Yelamanchili, S. V. Downregulation of an Evolutionary Young miR-1290 in an iPSC-Derived Neural Stem Cell Model of Autism Spectrum Disorder. *Stem Cell. Int.* **2019**, *2019*, 8710180.
(79) Shahjin, F.; Guda, R. S.; Schaal, V. L.; Odegaard, K.; Clark, A.; Gowen, A.; Xiao, P.; Lisco, S. J.; Pendyala, G.; Yelamanchili, S. V. Brain-Derived Extracellular Vesicle microRNA Signatures Associated with In Utero and Postnatal Oxycodone Exposure. *Cells* **2019**, *9*, 21.
(80) Ritchie, M. E.; Phipson, B.; Wu, D.; Hu, Y.; Law, C. W.; Shi, W.; Smyth, G. K. limma powers differential expression analyses for RNA-sequencing and microarray studies. *Nucleic Acids Res.* **2015**, *43*, No. e47.
(81) Metsalu, T.; Vilo, J. ClustVis: a web tool for visualizing clustering of multivariate data using Principal Component Analysis and heatmap. *Nucleic Acids Res.* **2015**, *43*, W566−W570.
(82) Bindea, G.; Mlecnik, B.; Hackl, H.; Charoentong, P.; Tosolini, M.; Kirilovsky, A.; Fridman, W.-H.; Pagès, F.; Trajanoski, Z.; Galon, J. ClueGO: a Cytoscape plug-in to decipher functionally grouped gene ontology and pathway annotation networks. *Bioinformatics* **2009**, *25*, 1091−1093.

https://dx.doi.org/10.1021/acsanm.0c01654
ACS Appl. Nano Mater. 2020, 3, 8906−8919